J Seismol
https://doi.org/10.1007/s10950-019-09866-7

ORIGINAL ARTICLE

Characterization of seismic signals induced by the operation of wind turbines in North Rhine-Westphalia (NRW), Germany

Tobias Neuffer · Simon Kremers · Ralf Fritschen

Received: 14 May 2019 / Accepted: 13 August 2019

Abstract In recent years, the impact of wind turbines (WTs) on seismological stations has been noticed, since WT-induced ground motions perturbed the seismic background noise level at seismological monitoring sites. The resulting deterioration of the recording quality at seismic stations leads to a conflict between seismological network and WT operators. As a first step towards the solution of the conflict - or at least a peaceful coexistence - it is of paramount importance to understand the characteristics of seismic signals generated by WTs. For this study, a 6.5-week measurement campaign was conducted at a wind park (WP) consisting of five 2 MW turbines in North Rhine-Westphalia (Germany) with eleven mobile seismic stations installed at distances of 1–10 km from the WP. At each measurement point, power spectral density (PSD) spectra are calculated and correlated with different operating states of the WTs. Changes in the operating states of the WT are reflected in the noise level at the seismic stations with different distances to the WP. An analysis of the radiated frequencies from the WT foundation into the subsurface is carried out by performing shutdown and switch-on tests at the WP. In this way, seismic signals generated by WTs are identified and used to illustrate how frequency-dependent peaks in WT-induced seismic noise are attenuated with distance. The attenuation of the peaks can be described by a power-law decay proportional to r^{-b}, with r as the distance between station and WT and b as the decay parameter with values between 2.4 and 5.5. The relationship between the noise level at a seismic station and the number of WTs in operation, that behave as interacting sources for the background noise level, could be determined as $\sim \sqrt{N}$, with N being the number of switched-on WTs.

Keywords Seismic noise · Wind turbine noise · Eigenfrequencies of wind turbine towers · Attenuation of seismic waves

1 Introduction

In North Rhine-Westphalia (NRW, Germany), a large number of seismological measurement stations are in operation for almost 40 years that are supervised by a wide variety of institutions such as universities, state offices, and service companies. The seismic networks of the individual operators can pursue various tasks that determine different requirements for stations within the network. For example, the seismic monitoring of geothermal plants or coal mining requires the recording of events that tend to be weak (Alber and Fritschen 2011). Therefore, stations of such a network

T. Neuffer (✉)
Ruhr-Universität Bochum, Universitätsstraße 150, 44780, Bochum, Germany
e-mail: tobias.neuffer@rub.de

S. Kremers · R. Fritschen
DMT GmbH, Co. KG, Am TÜV 1, 45307, Essen, Germany

Published online: 23 August 2019

are required to have very low (< 2 µm/s) background noise levels (Baisch et al. 2012) that are most likely achieved in non-urban areas. Those rural areas have also increasingly been used as locations to establish wind turbines (WTs), since the German government initiated the turnaround from fossil to renewable energies. This has caused a conflict between WT operators and institutions managing seismological networks, as the seismic noise generated by WTs has increased noticeably at nearby monitoring stations. In recent years, a number of studies have been published on the issue in which it is attempted to clarify the problems and conflicts. Styles et al. (2005) found that WTs produce characteristic signals depending for example on blade rotation velocity that can be observed in seismic recordings. A study by Stammler and Ceranna (2016) demonstrated that WT signals at seismic stations between 1 and 7 Hz become stronger with increasing wind speed and number of WTs. Furthermore, they discussed attenuation relations of WT signals with distance in different frequency bands, which can be described by a decay function of the type r^{-b}, with r as the distance between WT and seismic station and the attenuation factor b. Zieger and Ritter (2018) performed systematic measurements and were able to determine different frequency-dependent attenuation factors for near (< 100 m) and far field (> 100 m distance to WT). Saccorotti et al. (2011) demonstrated that WT signals with a peak frequency of 1.7 Hz could be detected at distances up to 11 km away from a wind park (WP). Even at a distance of 18 km, a WT signal with a peak frequency of about 4.3 Hz was identified, resulting in an amplitude attenuation proportional to r^{-1} (Schofield 2001).

Westwood and Styles (2017) analyzed the seismic wave field near a WT using polarization methods. They found the dominant wave types to be surface waves, mainly of Rayleigh type. The works of Gassenmeier et al. (2014) and Neuffer and Kremers (2017) used the Rayleigh wave-dominated wave fields in small frequency bands to determine the incidence directions of WT-induced signals to identify WP locations. Friedrich et al. (2018) went one step further and used seismic interferometry and migration methods to locate WTs as sources of continuous seismic signals. Furthermore, a clear distinction between WPs consisting of different WTs as different noise signals could be performed. Marcillo and Carmichael (2018) developed a method to detect fundamental frequency peaks and its harmonics of machines with rotating blades. They applied this method to two seismic stations and detected WT signals in agreement with the operational startup of WPs. The study by Gortsas et al. (2017) confirms the previous findings with numerical simulations based on the boundary element method and showed that (1) most of the seismic waves generated by WTs are radiated as Rayleigh waves, (2) the generated microseismic waves can affect seismic stations even in 15 km distance, and (3) higher perturbations are produced in a frequency range of 5–10 Hz compared with lower and higher frequency bands.

The objective of this study is to characterize the seismic signals that are generated by WTs and how different operating conditions of the turbine are affecting the ambient noise level at seismic stations in different distances. The influence of number, distance, and operational state of nearby WTs on seismic noise is investigated with different methods in the frequency-domain. This work is intended to contribute to a better understanding of the seismic signals emitted by WTs and the influence on the seismic background noise level.

2 Measurement campaign

As a part of a study to assess the disturbing effects of wind energy plants on seismological stations, the company DMT GmbH & Co. KG was commissioned by the "Ministry of Economic Affairs, Innovation, Digitalization and Energy of the State of North Rhine-Westphalia (MWIDE)" to conduct systematic measurements at a WP in Hilchenbach (NRW). The WP consists of five Enercon E-82 turbines with hub heights of 138 m, a rated power of 2 MW and three rotor blades per WT. The selected location possesses a 20-km radius free of additional WTs to prevent the influence of other WT-related vibration sources. Only one other WT with a hub height of 43 m and a rated power of 500 kW (established in 1995) is located within this radius. Since the dimensions of this WT are comparably small, the influence on the seismic noise level is neglected. In the proximity to the WP, ten measurement stations were placed in the field; five parallel and five perpendicular to the main wind direction in Germany (south-west to north-east) with logarithmic spaced distances to the WP starting at 1 km (Fig. 1,

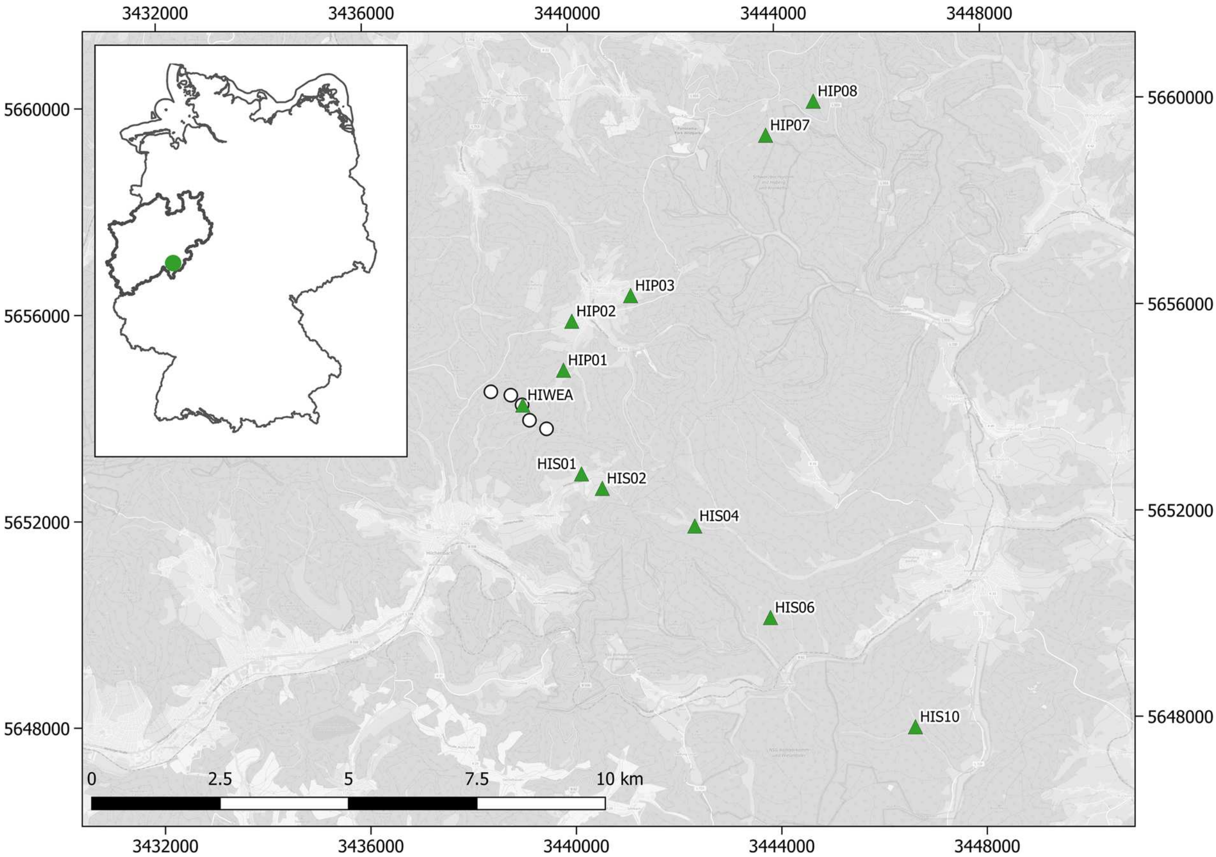

Fig. 1 The map shows the location of the Hilchenbach WP. The white dots show the WTs, the green triangles the installed seismic stations. The left map insert shows the location of the WP in NRW, Germany. OpenStreetMap contributors

Table 1). Additionally, one station was installed on the edge of the foundation of the central WT. The mobile stations continuously recorded the emitted vibrations for 6.5 weeks between March and April 2017 running autonomously on battery systems.

Table 1 Distance from the seismic measurement stations to the Hilchenbach WP. The given distances are measured in reference to the central WT

Station name	Distance to the central WT (m)
HIP01	1046
HIP02	1885
HIP03	2986
HIP07	7043
HIP08	8156
HIS01	1764
HIS02	2244
HIS04	4093
HIS06	6346
HIS10	9868

The instruments used for the mobile stations were a 4.5-Hz 3-component sensor with a 40-dB preamplifier and a SUMMIT M Vipa (DMT) digitizer. The internal instrument noise of the measurement chain is given as frequency-dependent power densities in Table 2, ranging below 10^1–10^4 times of the WT noise signals and is sufficiently low to allow analyzing the

Table 2 Frequency-dependent internal instrument noise of the measurement chain

Frequency [Hz]	Internal noise (nm^2/s)
1	< 1
3	< 10
5	< 5
7	< 15
10	< 20

radiated signals. The near-surface geology in the measurement area consists mainly of solid rock. Both the WTs and the ten surrounding measurement stations were located on clay and siltstone. The sensors were buried in 50 cm deep holes to protect them from wind and rain.

To identify the signals in the noise recordings that are exclusively caused by the operation of the WTs, shutdown and switch-on tests of the WTs were performed. These tests give an indication in the power and frequency content depending on the number of turbines in operation.

3 Data processing

The continuous data were recorded with 4.5-Hz geophones. In order to achieve a flat response to ground velocities from 1 Hz, the data were corrected to a geophone with a corner frequency of 0.8 Hz for the stations placed in the field. The recordings at the station that was installed on the tower foundation could be corrected to lower frequencies of 0.1 Hz, since the amplitudes of the input signals were much stronger compared with the signals measured in the field. The data were cut into 1-min segments as the WT data were made available by the WP operator in 1-min resolution. Power spectral density (PSD) spectra were calculated for each time segment, being binned and correlated to simultaneously recorded operational parameters of the WTs like wind speed, blade pass frequency (BPF, each of the three rotor blades passes the WT tower, which is three times the rotation rate) as a measure of the rotor velocity, output power, and hub azimuth as a measure of the wind direction. Afterwards, the interquantile mean between the 5 and 95% percentile (IQM95) of the PSD spectra of every operational state interval (bin) was calculated to reduce disturbing influences and outliers (Xi Engineering Consultants Ltd 2014). This results in one characteristic PSD curve for each selected correlation parameter of the WTs at all seismic stations. The PSD spectra are displayed in the frequency range of 1–10 Hz, which contains most of the dominant signal frequencies of local and regional seismic events (Bormann et al. 2013). WT-induced vibrations with higher frequency content are neglected as they experience higher attenuation along the propagation path (Lowrie 2007) and frequencies below approximately 1 Hz are dominated by marine-generated microseismicity (Friedrich et al. 1998). The processing procedure and data presentation has already been used and described in previous publications, such as Stammler and Ceranna (2016), Styles et al. (2005), Lott et al. (2017), Zieger and Ritter (2018), and Neuffer and Kremers (2017). To illustrate the results of the shutdown and switch-on tests, time-dependent PSD spectrograms were correlated with simultaneously recorded operational data of the WTs. As an additional intuitive value, root mean square (RMS) values over a frequency range of 3–8 Hz were calculated directly from the PSD spectra to move from frequency-dependent noise levels to an established value that is used to asses station quality (Groos and Ritter 2009).

4 Results

4.1 Correlated PSD spectra

For all stations, the recorded data of the vertical components were processed as described and the resulting PSD spectra were correlated with the prevailing wind speeds. Figure 2 shows the wind speed–correlated PSDs in a frequency range of 1–10 Hz for both profiles. The left column shows the PSD spectra at stations that were installed on the profile parallel to the dominating wind direction, the right column the PSD spectra for the perpendicular profile. The color of the curves represents the correlated wind speed. An increase of the noise level with increasing wind speed can clearly be observed in the frequency range from 3 to 8 Hz up to a distance of approximately 4.1 km (station HIS04). Distinct peaks between 3 and 4 Hz, 5 and 6 Hz, 6 and 7 Hz, and 7 and 8 Hz are visible, which decrease non-uniformly with increasing distances to the WP due to geometrical spreading, attenuation, and dispersion effects. At station HIS06 (6.3 km distance), slight wind-dependent peaks between 3 and 4 Hz are visible; whereas at higher frequencies, the noise level remains almost unchanged, independent on the wind speed. Stations HIP07 and HIP08 show weak broadband wind-dependent noise level increase; however, the distinct peaks observed at the closer stations are absent. The occurrence of these weak correlations can be explained by other wind-dependent noise sources such as trees in close vicinity to the stations. Especially for station HIP07, a generally increased noise

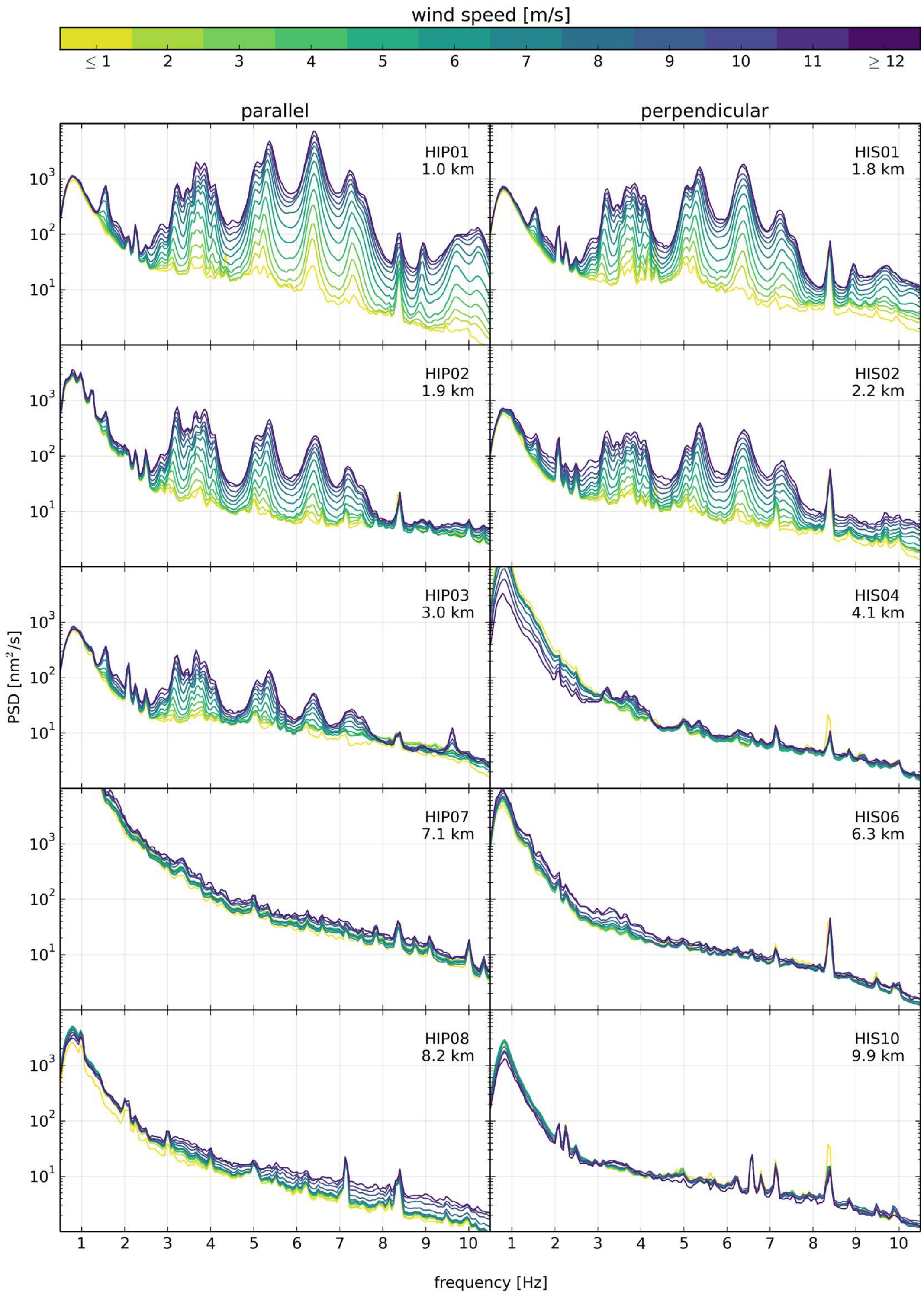

Fig. 2 Interquantile mean between 5 and 95% percentile (IQM95) of all PSD functions separated for wind speed for the vertical component of all ten stations in the proximity to the WP in Hilchenbach. Dark colors denote high, bright colors low wind speeds. The left column shows the spectra of the station profile parallel to the dominating wind direction in Germany. The right column shows the spectra for the perpendicular profile

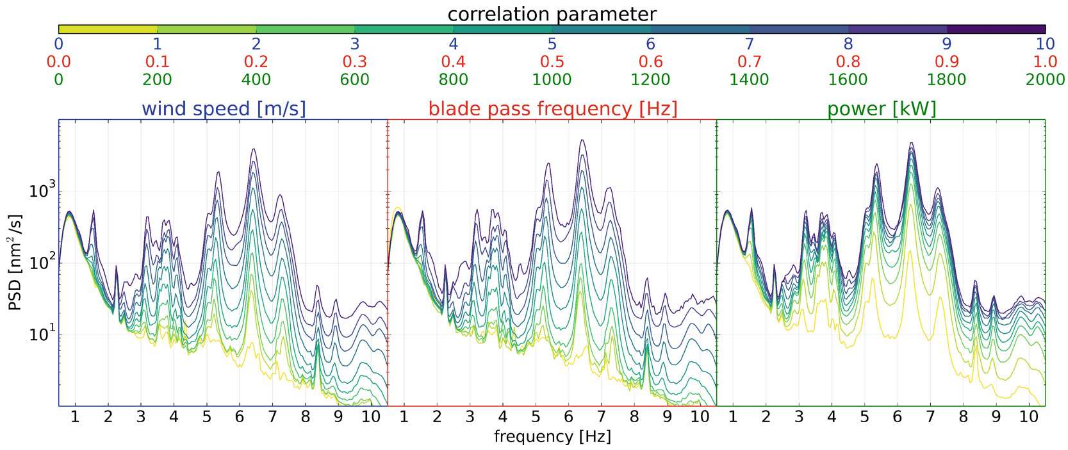

Fig. 3 PSD spectra separated for wind speed (left, blue frame), BPF (center, red frame), and power (right, green frame) at the vertical component of station HIP01. The colors of the labelling of the axis scale at the colorbar describe the bin limits of the respective correlation parameter (blue for wind speed, red for BPF, and green for power)

level over the whole PSD spectrum is noticeable, which is most prominent in very high spectral values for very low wind speeds ≤ 1 m/s compared with the values at the other stations during low wind times.

In Fig. 3, the PSD spectra of the vertical component at station HIP01 are correlated with different parameters. In the left blue framed part, the recorded wind speed in hub height, in the middle red framed part the blade pass frequency (BPF) of the central WT, and in the right green framed part the power of the central WT of the WP is used as correlation parameter. The number of bins is for all three correlation parameters the same, whereby the color of the axis scale labels under the colorbar shows the bin limits for the corresponding parameter (blue for wind speed, red for BPF, and green for power). Between the PSD spectra correlated with the wind speed and the spectra correlated with the BPF, significant differences are barely visible, since the rotation frequency of the rotor is linearly correlated with wind speed for this type of WT (Fig. 4, right). In contrast, the spectral amplitudes for low power values are higher compared with the amplitudes for low wind speeds, i.e., low BPFs. This can be explained by a difference in binning caused by the fact that even the lowest power values (200 kW) are generated starting from wind speeds of 2–3 m/s (the cut-in wind speed) or BPFs of 0.3–0.4 Hz (Fig. 4, left and middle). At the other end of the spectrum, the noise level rises insignificantly at high powers, since in the upper level, an increase of power towards the rated power is not achieved by increasing the rotor speed but by pitching the rotor blades close to the BPF limit.

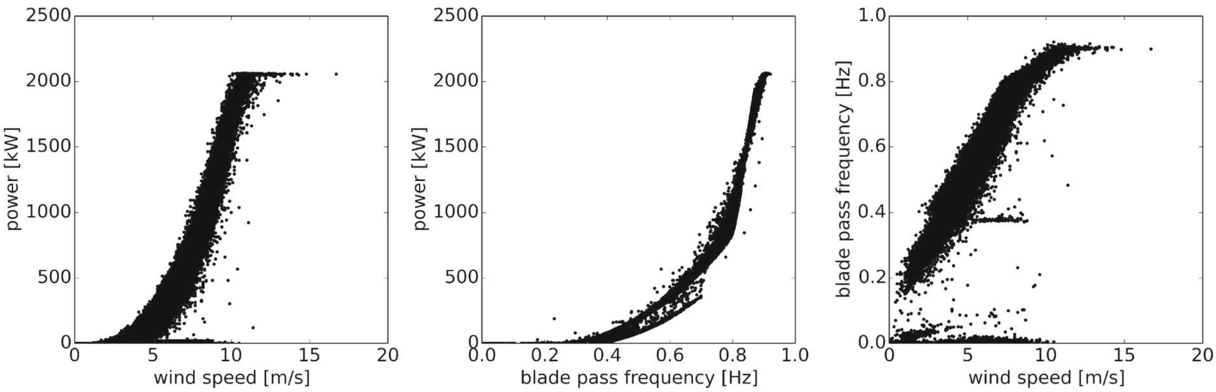

Fig. 4 The relation of the operating states to each other for the central WT of the WP in Hilchenbach over the entire measurement period. Left: power vs. wind speed. Middle: power vs. BPF. Right: BPF vs. wind speed

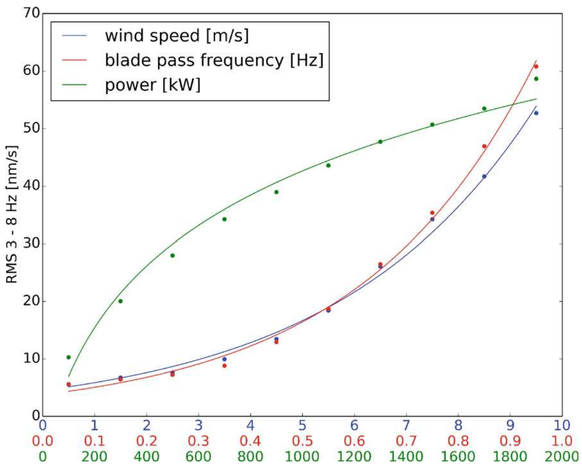

Fig. 5 RMS values between 3 and 8 Hz calculated from PSD spectra shown in Fig. 3. The colors of the labelling of the abscissa scale describe the bin limits of the respective correlation parameter (blue for wind speed, red for BPF, and green for power). The fitting curves show different characteristics depending on the correlation parameter

This does however not lead to a significant increase of the PSD values at station HIP01. Therefore, for this WT type, the turbine power is not a suitable correlation parameter to characterize the noise level at a seismic station caused by WT operation.

To further characterize the relationship between noise levels and the different operating conditions of the WTs, the mean ground velocity amplitudes in a given frequency band are correlated to the different WT operation parameters. Figure 5 shows RMS values between 3 and 8 Hz calculated from the PSD spectra at station HIP01 (Fig. 3) plotted against the correlation parameters. Again, color indicates the respective parameter (blue for wind speed, red for BPF, and green for power). Here the fitting curves for wind speed and BPF are similar, while the fit for the RMS values correlated with power shows a different characteristic. Wind speed and the linearly connected BPF seem to be the best correlation parameter to determine the influence parameter of the ground vibrations, since an increase of these operational parameters is directly accompanied by an increase of the noise level at the seismic stations.

The influence of the wind direction on the propagation characteristic of the waves induced by the WTs is assessed using polar diagrams (Fig. 6). Bins are created, which take into account both the azimuth of the hub position and the prevailing wind speed. Wind speed bins range from 0 to 10 m/s in 1 m/s step, whereas hub direction bins are divided into 45° steps. RMS values between 3 and 8 Hz are calculated for every bin and afterwards the interquantile mean between 25 and 75% percentile (IQM75) for every bin was determined. At this point, IQM75 values are calculated, since the database within the bins depends on two parameters and is therefore smaller compared with the PSD calculation as described before. This reduces the influence of strong outliers. Thus, one representative RMS value for a hub position and simultaneously measured wind speed is generated at the displayed seismic stations. The color scale shows the relative RMS normalized to the maximum and minimum of the corresponding station, where dark colors denote high and bright colors low noise conditions. Comparing the relative RMS values at high wind speeds between different hub positions reveal only minor differences. The stations HIP01 and HIP02 of the profile parallel to the main wind direction show slightly higher relative values if the hub position is in-line to the profile (W/SW–E/NE). The same applies to stations HIS01 and HIS02 of the profile perpendicular to the main wind direction. The RMS values at high wind speeds are higher at hub directions in-line to the profile (NW–SE) compared with other hub positions. The effect can be seen more clearly on the perpendicular profile (HIS01 and HIS02) than on the parallel profile (HIP01 and HIP02), which might be caused by the arrangement of the WTs in the WP. Considering the perpendicular profile (HIS01 and HIS02), the WTs are also in-line during periods with wind directions NW–SE with the station profile. This can lead to an increased superposition effect of the seismic waves radiated by the WTs for the perpendicular profile. However, in a comparison of the impact factors that are influencing the strength of the radiated noise field, the wind direction seems not to be a key parameter.

4.2 Shutdown tests and tower foundation measurements

An identification of signals in the noise recordings that are exclusively generated by the operation of the WTs was performed by shutdown and switch-on tests of the WTs for several hours. The tests were started on short notice based on detailed weather forecasts.

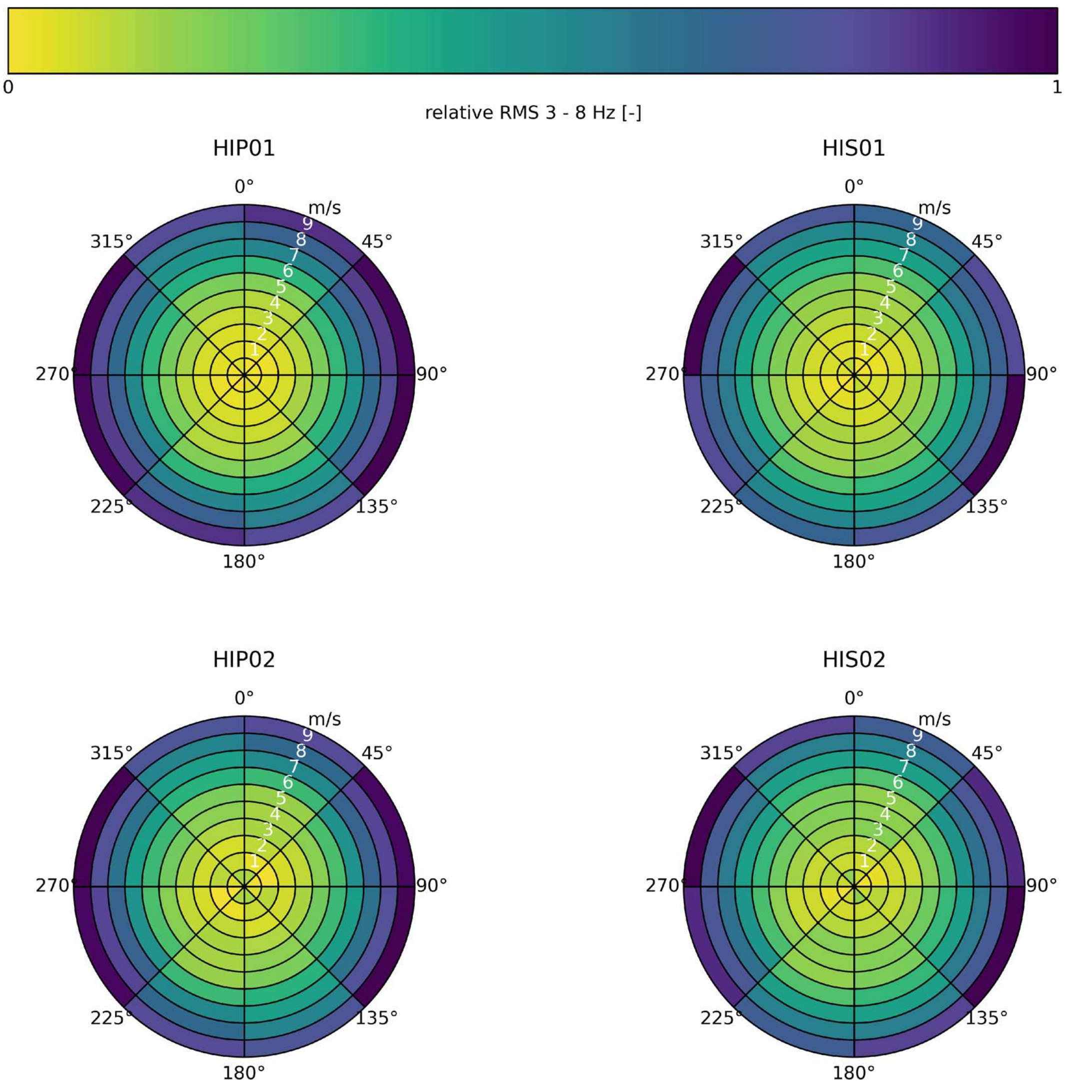

Fig. 6 Polar diagrams to evaluate the influence of the wind direction on the noise level at the stations HIP01, HIP02, HIS01, and HIS02. The radial axes indicate the prevailing wind speed, with the individual angular axes showing the azimuth of the WT hub. For each wind speed/azimuth bin, the interquantile mean between 25 and 75% percentile of all calculated RMS values between 3 and 8 Hz was determined. The color scale denotes the relative RMS value, normalized to the minimum and maximum of the corresponding station

Figure 7 shows a shutdown test over 12 h, while all five WTs of the WP were switched off and in trundling mode. PSD spectrograms of the stations HIWEA that was placed on the foundation of the central WT and HIP01 in about 1 km distance are shown, as well as the wind speed and BPF recordings of the WT at the same time. The abscissa of the spectrograms represent time, the ordinate the frequency, and the color scale PSD amplitudes. Immediately after shutting down the WTs, the noise level decreases at both stations. Vice versa, the noise level at both stations immediately increases after switching on the WTs. The spectrogram of station HIWEA shows that, while the WT is switched off, mainly the same discrete frequencies are visible in the PSD spectra, which are also visible during operation, but with significantly lower amplitudes. Single narrow-band peaks in the PSDs during switch-off times (e.g., between 1 and 2 Hz, 5 and 6 Hz, 6 and 7 Hz) are broadening and merging to one frequency peak after the WT has been switched on. This

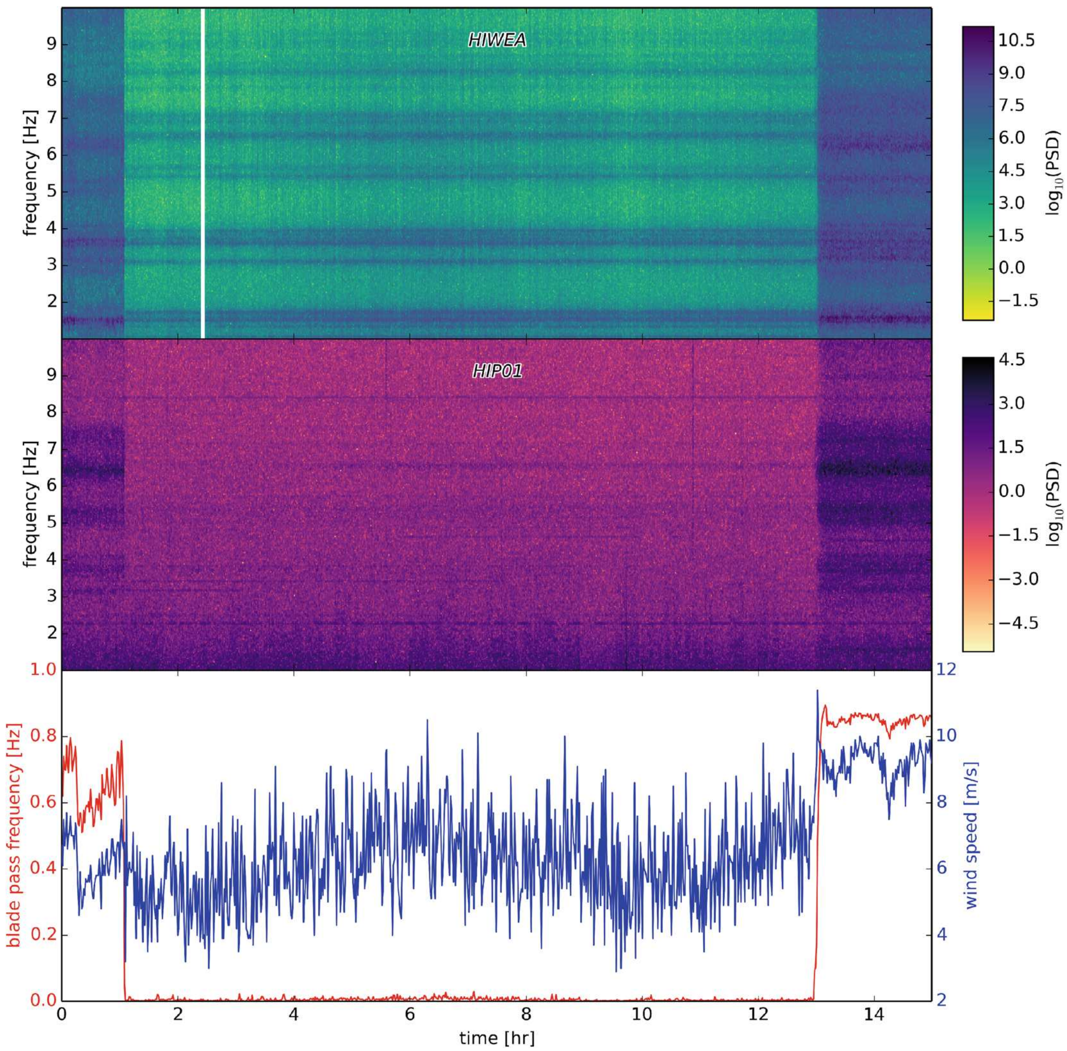

Fig. 7 PSD spectrograms of two stations over 15 h during which a shutdown test was performed. The spectrograms show the frequency-dependent PSD spectra in 1-min resolution. The abscissa represents time, the ordinate the frequencies, and the color scale the amplitudes of the PSD spectra. The bottom diagram shows the recorded correlation parameters at the same time (blue for wind speed and red for BPF of the central WT)

observation suggests that the discrete frequency peaks during operation are the eigenfrequencies and their harmonics of the tower recorded on the foundation superimposed and excited by the BPF harmonics. Moreover, seismic energy of additional frequency bands at the foundation can be detected during operation that are allocated to the BPF harmonics. However, only peaks that can be related to the eigenfrequencies of the tower are present in the PSD spectra at the seismic stations in the field, which indicates that by running a WT, the natural frequencies of the tower and its harmonics are transmitted through the foundation into the subsurface. Moreover, it can be noted that during the switch-off time, the excitation of the natural frequencies of the tower by trundling and wind load are of such weak strength that these frequencies are almost absent in the spectra of station HIP01 that is installed in the field. However, a slight increase of the noise level between 6–7 Hz and 8–9 Hz compared with the rest of the displayed frequency range can be observed.

A detailed view on the recording of station HIWEA at the tower foundation is given in Fig. 8, showing a PSD spectrogram recorded at the central WT over

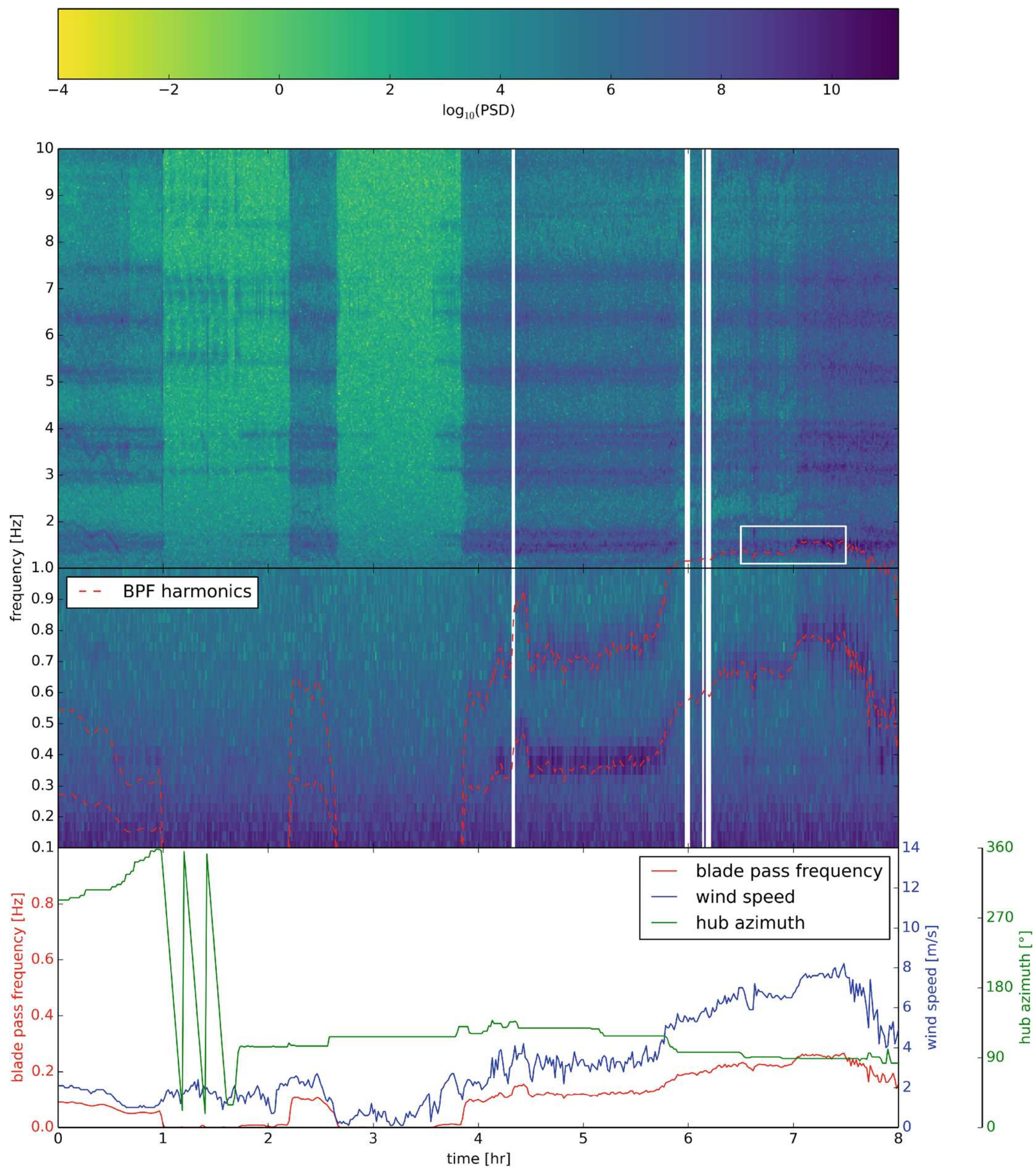

Fig. 8 PSD spectrogram of the station on the WT foundation over 8 h. The spectrogram shows the frequency-dependent PSD spectra in 1-min resolution. The abscissa indicates the time, the ordinate the frequencies, and the color scale the amplitudes of the PSD spectra. The upper part of the spectrogram shows the frequency range of 1–10 Hz, the lower part the range of 0.1–1 Hz. The bottom diagram shows the recorded correlation parameters at the same time (blue for wind speed, red for BPF, and green for hub azimuth of the central WT). An explanation of what the white box represents can be found in the text

8 h. The upper part of the spectrogram illustrates the frequency range from 1 to 10 Hz, the lower part the range from 0.1 to 1 Hz. The color scale denotes the amplitudes in the PSD spectra. Additionally, the wind speed, BPF, and hub direction during the recording time are given below the spectrogram. As soon as the rotor blades are turning, the natural frequencies and harmonics can be measured at the foundation. The periods around hour 1.5–2 and hour 3.5–4 show that with slight trundling of the rotor blades, the natural frequencies of the tower are stronger excited, compared with total stagnation. In addition, at hour

1–1.75, the constant untwisting of the hub leads to an excitation of diffuse frequency bands. The natural frequencies and harmonics of the tower are not predominantly excited during this process. However, it is noticeable that as soon as the WT starts operation, peaks in the PSD spectrogram are present in the range of the natural frequencies and harmonics of the tower at the foundation. Furthermore, the harmonics of the BPF can be detected in the spectrogram between 0.1 and 1 Hz at the foundation starting from hour 4, while the WT is switched on. The frequency peaks in the spectrogram show the exact BPF indicated by the dark colors of the spectrogram and the red dashed line representing the BPF and their harmonics. At higher frequencies between 1 and 5 Hz, the higher harmonics of the BPF are observable in the PSDs (hour 6–7). If the harmonics of the BPF match the eigenfrequencies of the tower within the frequency range of 1–5 Hz, the PSD peaks at the foundation are slightly amplified. This is, for example, visible in the time span between hour 6.5 and 7.5, where the BPF harmonics match the tower eigenfrequencies of about 1.5 Hz (see white box in Fig. 8).

A detailed assessment of the BPFs measured at the seismic station on the foundation in the frequency range of 0.1–2 Hz is shown in Fig. 9. In the upper part (Fig. 9a, b), PSDs of the vertical component of the station HIWEA correlated to the BPF of the WT are shown. In both cases (a and b), the PSDs are the same, while the color scale in (a) represents the recorded BPF of the WT and in (b) the first harmonic of the BPF. The first tower eigenfrequency is 0.35 Hz, since a discrete peak remains constant independent of the BPF (Wörmann and Harte 2005). At approximately 1.5 Hz, a peak can also be detected, which does not vary in frequency but only in amplitude, indicating the second eigenfrequency of the tower. In the frequency range from 0.4 to 1.0 Hz, peaks are visible, which are shifted to higher frequencies in the PSD spectrum with increasing BPF. Moreover, the peak shifted with increasing BPF also increases in amplitude. Figure 9c shows the correlated PSD spectra

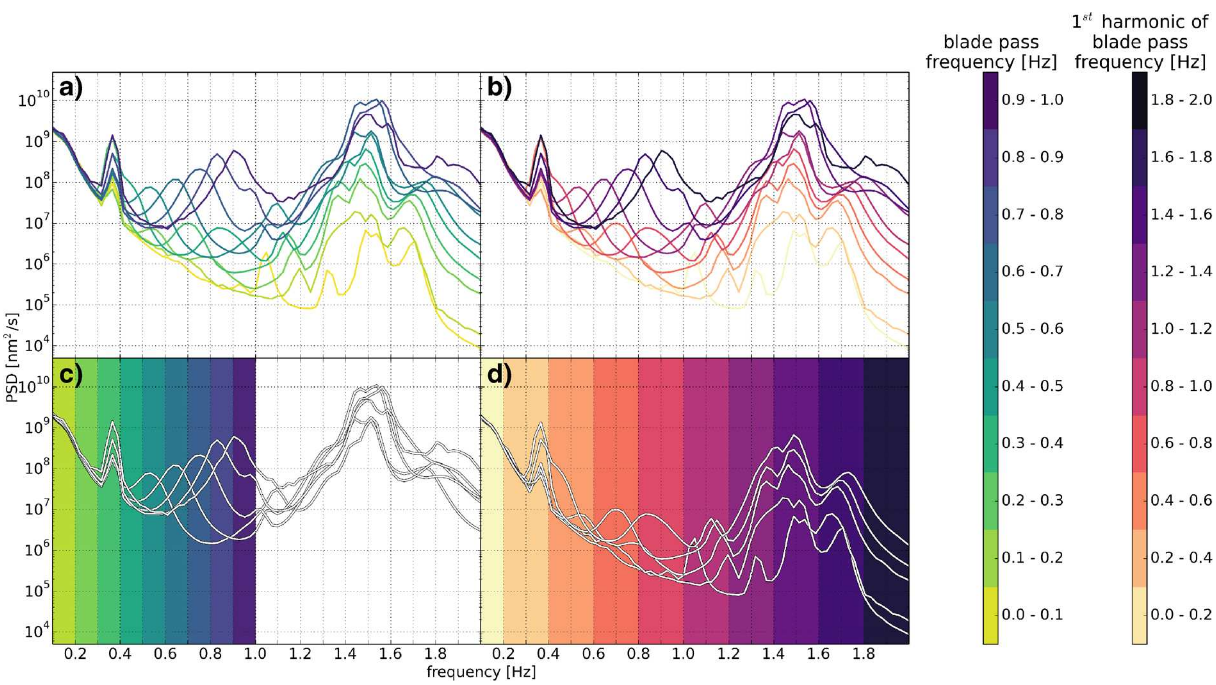

Fig. 9 PSD spectra of the seismic station HIWEA installed on the foundation of the central WT of the vertical component in the frequency range 0.1–2 Hz separated for BPF. **a** The color scale indicates the BPF. **b** The color scale indicates the first harmonic of the BPF. **c** The correlated PSD spectra for BPFs between 0.5 and 1.0 Hz (green to blue in (**a**) or red to purple colored lines in (**b**)) with colored frequency bands representing the BPF. **d** The correlated PSD spectra for BPFs between 0.1 and 0.5 Hz (yellow to green in (**a**) or yellow to red colored lines in (**b**) with colored frequency bands representing the first harmonic of the BPF

for BPFs between 0.5 and 1.0 Hz (here the unit Hz refers to rotation speed of the rotor and should not be confused with the frequency content of the PSDs) as white curves. The colored sections highlight frequency bands that refer to the correlated BPF bins. It can be seen that the PSD amplitude peaks lie exactly in the highlighted frequency bands of the BPF. The same applies to the first harmonic of the BPF. Figure 9d shows the correlated PSDs for low BPFs between 0.1 and 0.5 Hz (again Hz refers to the blade rotation speed) as white curves. Again, the peaks lie exactly in the highlighted frequency bands of the first harmonic of the BPF. Thus, the movement of the rotors of the WT is reflected as frequency peaks in the vibration measurements recorded at the tower foundation. Apparently, the rotor speed is controlled in such a way that the BPF does not match the first and second eigenfrequency of the tower during operation at times when power is generated to prevent the excitation of resonant vibrations (Harte and Van Zijl 2007). The peaks generated by the BPF range from approximately 0.4–1.0 Hz, whereas the eigenfrequencies lie directly below (0.35 Hz) and above (1.5 Hz) this range. However, harmonics of the BPF coincide with higher harmonics of the tower eigenfrequencies. Therefore, these frequencies are increasingly excited, radiated via the foundation into the subsurface and measured at the seismic stations in the field (see figures above). The signals generated by the blade rotation are not observable at the seismic stations in the proximity to the WTs, presumably caused by a superposition of marine-generated microseismicity below 1 Hz and by the resolution capability of the used equipment.

4.3 Attenuation of PSD peaks and superposition effects

The wind speed–correlated PSD spectra at the seismic stations (Fig. 2) allow to determine frequency-dependent amplitude decay relationships. Since a directional dependence of the noise level could barely be detected (Fig. 6), the stations of the parallel and perpendicular profile are used as a combined dataset to estimate the attenuation behavior of the various frequency peaks. Figure 10 shows differential PSD values with the difference obtained from the peaks at strong wind conditions ($\geq$ 12 m/s) and weak wind conditions ($\leq$ 1 m/s), plotted against the distance between the station and the central WT. PSD peak differences are used to exclude station specific noise effects that are not caused by the operation of WTs. Decay relations for PSD peaks, which are identified in Fig. 2 as clearly WT induced, are determined in different frequency bands of 3.0–3.3 Hz, 3.5–4.0 Hz, 5.0–5.2 Hz, 5.2–5.5 Hz, 6.3–6.6 Hz, and 7.1–7.4 Hz. The relation of the attenuation of the peaks can then be described by a power-law decay proportional to r^{-b}, with distance between station and WT r and the decay parameter b (Stammler and Ceranna 2016). With increasing frequencies, the b values increase, i.e., the attenuation is stronger at higher frequencies, ranging between 2.4 and 5.5 for the different frequency bands. Assuming that the WT as a point source emits mainly surface waves, the geometrical spreading of the waves as it can be found in literature can be described as $\sim r^{-1}$ in “PSD domain”. However, the determined decay of the PSD peaks are higher due to frequency-dependent damping and geometric scattering effects.

The retrieved decay relationships apply to the case that all five WTs are in operation, since it can be assumed that all five WTs are switched on under strong wind conditions. This means that five independent sources are transmitting vibrations into the ground leading to superposition effects of the radiated waves by WTs in the closer proximity to the WP. In order to investigate this effect in more detail, a switch-on test was conducted. All WTs were first switched off and successively switched on in 10 min intervals. Figure 11 illustrates the noise level behavior during the switch-on test. The spectrogram shows the frequency- and time-dependent PSD values at station HIP01, while the color scale describes the amplitudes of the PSD spectrum. The middle section gives the corresponding calculated RMS value over a frequency range of 3–8 Hz, while the bottom section shows the BPFs of the WTs, which are switched on successively. The colored lines denote the times when the respective WT is switched on. As soon as all WTs are switched off, the seismic noise drops to an almost constant level over the complete frequency band, independently from wind speed. When the first WT is switched on, the characteristic frequency peaks are immediately observable in the spectrogram. Switching on further WTs causes an amplification of these frequency peaks, whereby the frequencies remain the same. Considering the RMS value at the switch-on times of the WTs, it can be recognized that it rises

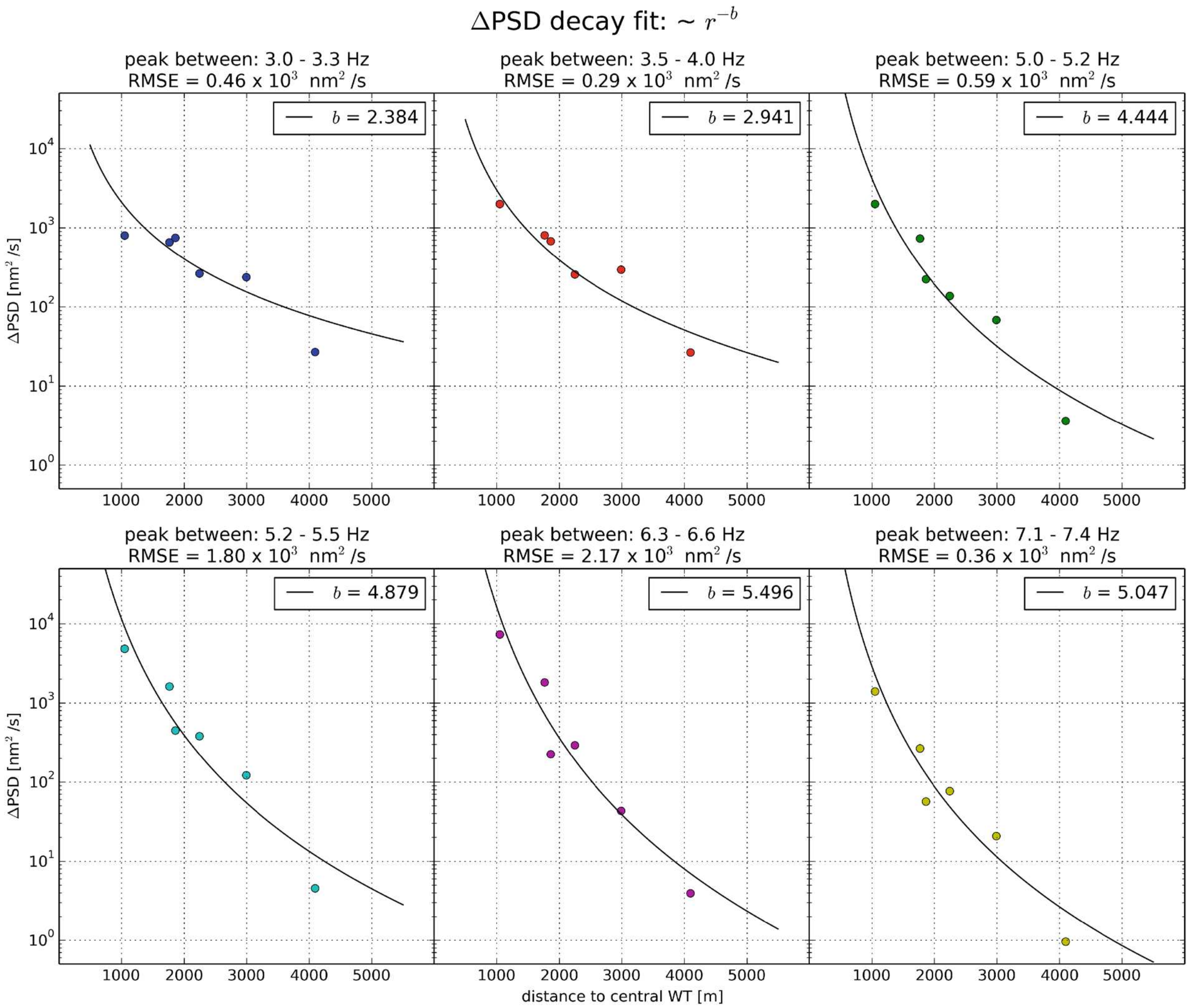

Fig. 10 Amplitude decay relationships for differential PSD peaks with distance for different frequency bands. The *Δ*PSD values describe the difference of the PSD amplitudes at strong wind ($\geq$ 12 m/s) and weak wind ($\leq$ 1 m/s) for the stations HIP01, HIP02, HIP03, HIS01, HIS02, and HIS04 with the respective distances to the central WT of the WP. A power-law decay proportional to r^{-b} is fitted to the data

with increasing number of WTs, but is additionally dependent on the BPFs.

The determination of the relationship between the noise level at station HIP01 and the number of WTs in operation is demonstrated in Fig. 12. The crosses represent the RMS values between 3 and 8 Hz, which are computed every minute for 10-min periods with a constant number of WTs in operation (Fig. 11). For example, the blue crosses show the RMS values calculated between minutes 70 and 80 in 1 min resolution during the time when three WTs are in operation. The arithmetic mean of these values is divided by the average BPF of the three WTs that are switched on during that period. This value is again divided by the average BPF of all WTs over the entire period of the switch-on test in order to determine a weighted average and to eliminate the dependence on the BPF with the intention to only asses the influence of the number of WTs on the superposition effects. This results in one representative value per switched-on WT (colored dot). The fitting curve (black line) can be written as $\sim N^{0.598} \approx \sqrt{N}$, with N as the number of WTs in operation. This

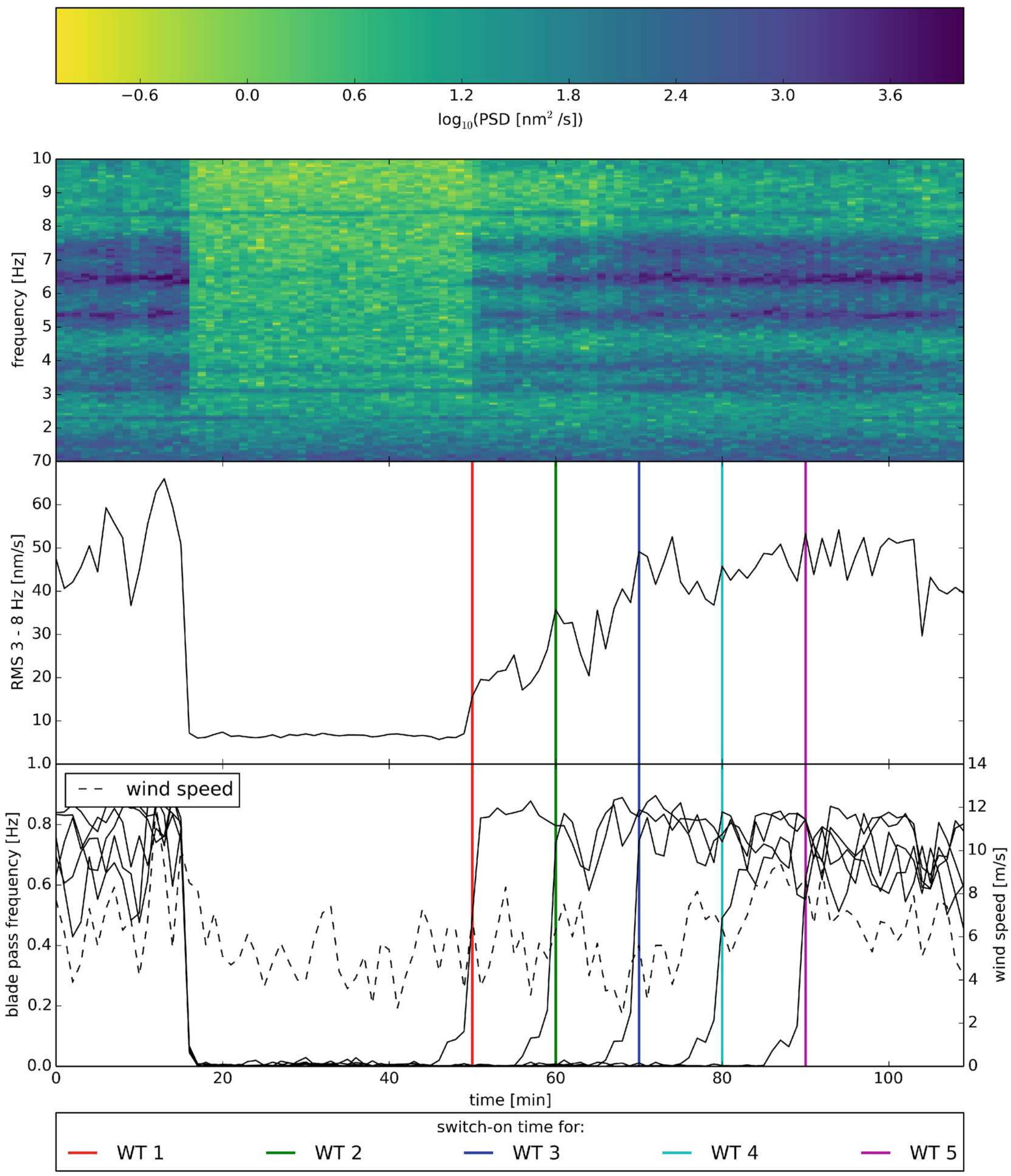

Fig. 11 PSD spectrogram at station HIP01 during the switch-on test at the WP. The upper section shows a frequency and time-dependent spectrogram over almost 2 h. The middle section shows the corresponding calculated RMS value between 3 and 8 Hz at the same time. The lower section shows the BPFs of the five WTs. Color marked are the times when the respective WT is switched on

means that the impact on the background noise level due to the operation of N WTs adds up proportional to $\sqrt{N}$. This relation is in agreement with previous findings in studies by Styles et al. (2005), Schofield (2001), and Neuffer and Kremers (2017).

5 Discussion

The objective of this work is to characterize seismic signals induced by the operation of WTs. As already shown in other studies, clear WT-related PSD peaks in

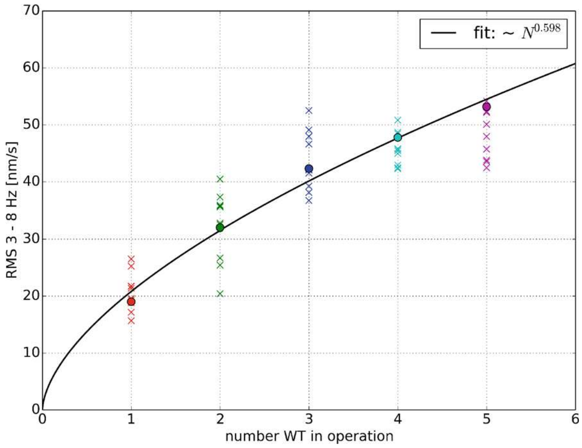

Fig. 12 Relationship between the noise level at station HIP01 and the number of WTs in operation. The crosses represent the RMS values between 3 and 8 Hz, which are computed every minute for periods with a constant number of WTs in operation (Fig. 11). The dots represent a weighted average of the RMS values (crosses). The black line illustrates the fitting curve to the weighted average values

a frequency range of 1–10 Hz can be identified, which increase in amplitude with increasing wind speed and BPF of the nearby WTs. The correlation of PSD spectra at the seismic stations with wind speed yields very similar results as correlating with the BPF. This is due to the linear relationship between wind speed and BPF (Fig. 4) that was observed for the investigated WT type (Enercon E-82). The characteristic WT signals can be identified at seismic stations up to a distance of about 5 km. The frequency-dependent decay relations of the PSD peaks can be described as r^{-b}, with distance to the WT r and attenuation factor b. The b value lies in the range from 2.4 to 5.5 depending on the peak frequencies. Other studies such as Stammler and Ceranna (2016), Styles et al. (2005), and Zieger and Ritter (2018) find different values, originating in different geological conditions and WT types that were investigated in these studies. In particular, we assume that the different WT types should be regarded as different sources for radiated seismic waves due to different construction and foundation types. The emitted waves strongly depend on WT type, whereas the attenuation depends on ray path and thus on the geology with different attenuation properties. Xi Engineering Consultants Ltd (2014) presumed that the noise levels for stations in-line with wind direction to the WT are higher compared with stations installed in cross-wind direction. A minor directional dependence could also be identified in this study (Fig. 6). The stations HIS01 and HIS02 show a slightly higher noise level, if the wind direction is parallel to the azimuthal orientation of the stations to the WT. However, a stronger superposition of the emitted waves might be caused by the geometric arrangement of the WTs in the WP regarding to the position of the seismic stations. The comparison between measurements at the WT foundation and measurements in the field, especially during shutdown tests at the WP, indicates that the dominant frequency peaks in the PSD spectra related to WT signals describe the eigenfrequencies and the harmonics of the turbine tower. Other studies such as Styles et al. (2005) and Westwood et al. (2015) have shown that BPFs and their harmonics also emerge as peaks in the spectra at seismic stations installed in the field close to WTs. These studies dealt with the investigation of fixed-speed machines. Therefore, a shift of the frequency peaks in PSD spectra with increasing wind speed could not be detected, since the rotation rate of the rotor blades is constant. Similarly, Schofield (2001) identified varying frequencies at the base of a turbine tower, that can also be related to rotation frequencies and harmonics of the investigated turbine type, which stabilize with increasing wind speed, because of the WT design to run at a nearly constant rotation rate. In contrast, our analysis focuses on WTs with variable rotation speed design, with similar results being found in the data recorded on the tower foundation. The changing BPF is directly visible in the PSD spectra of the foundation data. However, no indication for this behavior could be observed in the data recorded at the seismic stations in the field starting from 1 km distance. This finding is supported by the results presented in Fig. 3 that demonstrated the constant frequency of dominant peaks in the PSD spectra. The origin of the frequency peaks that can be detected at the seismic stations in the field are therefore believed to be the eigenfrequencies and their harmonics of the tower superimposed and excited by the BPF and its harmonics. In order to quantify the superposition effects of several WTs, switch-on tests were conducted at the WP, where the WTs were successively switched on in 10-min steps. The results show that the noise level at the seismic stations increases as a function of the number of WTs with the factor $\sqrt{N}$, with N as the number of WTs in operation. The studies of Styles et al. (2005) and Neuffer and Kremers (2017) describe comparable superpositions. Stammler and Ceranna (2016) presented an amplification factor due to superposition effects using squared values of the ground velocity (PSD with units nm^2/s) resulting in factor N, corresponding to $\sqrt{N}$ when converted into RMS values.

6 Conclusion

Based on 6.5 weeks of continuous seismic recordings in the vicinity to a WP in Hilchenbach, NRW, Germany, WT signals and their characteristics were investigated. Ten measurement stations were installed in the field at distances between 1 and 10 km from the WP, whereas prominent PSD peaks, which increase in amplitude with increasing wind speed or BPF, are clearly detectable up to distances of approximately 4–5 km. By performing shutdown tests and measurements at WT foundation, it could be verified that dominant PSD peaks in the frequency range of 1–10 Hz at the measurement stations reflect the eigenfrequencies and harmonics of the WT tower. The attenuation of the frequency-dependent PSD peaks with distance to the WP can be described as r^{-b}, with r as the distance between seismic station and WT and b as the attenuation factor. The b values range from 2.4 to 5.5, with higher values for higher frequencies. Furthermore, it could be shown by conducting switch-on tests, during which WTs of a WP were successively taken into operation, that superposition effects of the noise level can be described as proportional to $\sqrt{N}$, with N as the number of WTs in operation.

Acknowledgments The authors are grateful to the "Ministry of Economic Affairs, Innovation, Digitalization and Energy of the State of North Rhine-Westphalia (MWIDE)," "EnergieAgenturNRW," and "Landesamt für Natur, Umwelt und Verbraucherschutz (LANUV NRW)" for the permission to use the seismic data recorded within the scope of the commission. We also thank "Enercon GmbH" for providing operational data of the wind turbines and the permission to publish. We would like to thank the Hilchenbach wind park operators and the owners of the sites on which the mobile seismic stations were installed during the measurement campaign. Finally, we also would like to thank the editor and the anonymous reviewer for their recommendations that greatly improved this work.

References

Alber M, Fritschen R (2011) Rock mechanical analysis of a M1 = 4.0 seismic event induced by mining in the Saar District, Germany. Geophys J Int 186(1):359–372

Baisch S, Fritschen R, Groos J, Kraft T, Plenefisch T, Plenkers K, Ritter JRR, Wassermann J (2012) Empfehlungen zur Überwachung induzierter seismizität-positionspapier des FKPE. DGG Mitteilungen 2012(3):17–31

Bormann P, Wendt S, DiGiacomo D (2013) Seismic sources and source parameters. New manual of seismological observatory practice 2 (NMSOP2). Potsdam:, Deutsches GeoForschungsZentrum GFZ:1–259

Friedrich A, Krueger F, Klinge K (1998) Ocean-generated microseismic noise located with the gräfenberg array. J Seismol 2(1):47–64

Friedrich T, Zieger T, Forbriger T, Ritter JR (2018) Locating wind farms by seismic interferometry and migration. J Seismol 22(6):1469–1483

Gassenmeier M, Sens-Schönfelder C, Delatre M, Korn M (2014) Monitoring of environmental influences on seismic velocity at the geological storage site for CO2 in Ketzin (Germany) with ambient seismic noise. Geophys J Int 200(1):524–533

Gortsas TV, Triantafyllidis T, Chrisopoulos S, Polyzos D (2017) Numerical modelling of micro-seismic and infrasound noise radiated by a wind turbine. Soil Dyn Earthq Eng 99:108–123

Groos J, Ritter J (2009) Time domain classification and quantification of seismic noise in an urban environment. Geophys J Int 179(2):1213–1231

Harte R, Van Zijl GP (2007) Structural stability of concrete wind turbines and solar chimney towers exposed to dynamic wind action. J Wind Eng Ind Aerodyn 95(9-11): 1079–1096

Lott FF, Ritter JR, Al-Qaryouti M, Corsmeier U (2017) On the analysis of wind-induced noise in seismological recordings. Pure Appl Geophys 174(3):1453–1470

Lowrie W (2007) Fundamentals of geophysics. Cambridge university press

Marcillo OE, Carmichael J (2018) The detection of wind-turbine noise in seismic records. Seismol Res Lett 89(5):1826–1837

Neuffer T, Kremers S (2017) How wind turbines affect the performance of seismic monitoring stations and networks. Geophys J Int 211(3):1319–1327

Saccorotti G, Piccinini D, Cauchie L, Fiori I (2011) Seismic noise by wind farms: a case study from the Virgo Gravitational Wave Observatory, Italy. Bull Seismol Soc Am 101(2):568–578

Schofield R (2001) Seismic measurements at the stateline wind project. Rept No LIGO T020104-00-/, Laser Interferometer Gravitational Wave Observatory available at http://www.ligocaltechedu/docs

Stammler K, Ceranna L (2016) Influence of wind turbines on seismic records of the gräfenberg array. Seismol Res Lett 87(5):1075–1081

Styles P, Stimpson I, Toon S, England R, Wright M (2005) Microseismic and infrasound monitoring of low frequency noise and vibrations from windfarms. Recommendations on the Siting of Windfarms in the Vicinity of Eskdalemuir, Scotland, Report to MOD/FTI/BWEA, pp 125

Westwood RF, Styles P, Toon SM (2015) Seismic monitoring and vibrational characterization of small wind turbines: a case study of the potential effects on the Eskdalemuir International Monitoring System Station in Scotland. Near Surface Geophysics 13(2):115–126

Westwood RF, Styles P (2017) Assessing the seismic wavefield of a wind turbine using polarization analysis. Wind Energy 20(11):1841–1850

Wörmann R, Harte R (2005) Vorgespannte betontürme für windenergieanlagen: einflüsse nichtlinearer Materialeigenschaften auf die Eigenfrequenzen als Entwurfskriterium. Beton-und Stahlbetonbau 100(7):549–560

Xi Engineering Consultants Ltd (2014) Seismic vibration produced by wind turbines in the Eskdalemuir region. Release 2.0 of Substantial Research Project, Xi Engineering Consultants Conference House, 152 Morrison Street, Edinburgh, EH3 8EB, xiengineering.com

Zieger T, Ritter JR (2018) Influence of wind turbines on seismic stations in the upper rhine graben, SW Germany. J Seismol 22(1):105–122